Ultra-Thin Highly Deformable Composite Mirrors

John Steeves* and Sergio Pellegrino†
California Institute of Technology, Pasadena, CA 91125

Optical quality mirrors are heavy, expensive and difficult to manufacture. This paper presents a novel mirror concept based on an active laminate consisting of an ultra-thin carbon-fiber shell bonded to a piezo-ceramic active layer coated with patterned electrodes. Mirrors based on this concept are less than 1 mm thick and hence are very lightweight and flexible. They also have a large dynamic range of actuation that allows them to take up a wide range of deformed configurations. This concept is compatible with relatively high-volume manufacturing processes and can potentially achieve a significant reduction in cost in comparison to currently available active mirrors. It is also suitable for applications ranging from concentrators for solar power generation to primary mirrors for optical telescopes.

The paper presents an overview of the mirror components as well as a simple design relationship for sizing the active layer. The expected performance of a preliminary design for a 1 m diameter mirror with a radius of curvature of 15 m is computed numerically, showing that a set of 96 actuators can remove an edge-to-edge manufacturing-induced cylindrical curvature of 5 mm to an RMS accuracy of 50 μm. The prescription of the mirror can also be adjusted to a radius of curvature of 11 m with an accuracy of 160 μm. The development and characterization of a proof-of-concept prototype mirror is also presented.

I. Introduction and Background

Large mirrors have a wide range of applications, including the collection of photons to study distant stars and planets, space-based Earth imaging, and solar power concentration for the production of alternative energy. All of these applications will benefit from the development of technologies to mass produce very precise large mirrors at low cost. In astronomy, where tight requirements on figure error and surface quality are encountered, the trend is towards thinner and lighter structures whose shape is measured and controlled by means of actuators. In only 20 years the state of the art has moved from the Hubble Space Telescope primary mirror, made by grinding and polishing a "blank" of near-zero coefficient of thermal expansion (CTE) glass, which was entirely passive and had an areal density of $\sim$ 180 kg/m^2,[1] to the lightweight segments of the James Webb Space Telescope[2] primary mirror, weighing $\sim$ 25 kg/m^2 each. These segments are active in nature, containing a small number of actuators that are used to control position, orientation and overall curvature. Even further developments have been made in order to construct adaptive primary mirrors consisting of a silicon carbide structure supporting a precision optical face-sheet, whose shape is controlled by actuators embedded in the support structure.[3] These latest mirrors, weighing $\sim$ 10 kg/m^2, are still relatively heavy and also involve complex manufacturing processes, rendering them expensive and slow to produce.

A novel approach to address these issues has been proposed by our group and collaborators at Caltech and JPL.[4–6] In this concept an active laminate consisting of a stiff substrate with an optical quality reflective surface bonded to layers of piezoelectric material covered with patterned electrodes, has been demonstrated for 10 cm diameter mirrors for the Autonomous Assembly of a Reconfigurable Space Telescope (AAReST) project (see http://pellegrino.caltech.edu/aarest.html for more details). The next step in the development of potentially low-cost, large lightweight mirrors is the scaling up of this concept: this is the objective of the present study.

*Graduate Student, Graduate Aerospace Laboratories, 1200 E. California Blvd. MC 105-50. jsteeves@caltech.edu
†Joyce and Kent Kresa Professor of Aeronautics and Professor of Civil Engineering, Graduate Aerospace Laboratories, 1200 E. California Blvd. MC 301-46. AIAA Fellow. sergiop@caltech.edu

We have chosen to focus on mirrors for light collection and/or concentration. As these are non-imaging applications, the tolerances on the required mirror figure are significantly less stringent. One such example of a light-collecting system is that of solar concentrators. Solar concentrators use parabolic-shaped mirrors to produce a highly concentrated spot of light which is then used for power generation via 1) photovoltaic cells or 2) heat engines. Currently, several methods have been developed in order to produce low-cost mirrors for these systems. These range from glass slumping, injection molding of polymers, and even inflatable balloon-type structures.[7–9] However, there are a number of disadvantages common to these methods. The most prominent of these is that the mirrors have no corrective capabilities. This ultimately makes them susceptible to errors introduced during installation and also due to external disturbances during operation (e.g. wind loading). Errors such as these ultimately degrade the capability of the concentrator, thus reducing the efficiency of the solar concentrating system as a whole.

For this application, we have developed an alternative version of the active laminate mirror, consisting of an ultra-thin carbon-fiber shell bonded to a piezo-ceramic active layer. Mirrors based on this concept are less than 1 mm thick and hence are very lightweight and flexible. They also have a large dynamic range of actuation that allows them to take up a wide range of deformed configurations. This concept is compatible with relatively high-volume manufacturing processes and can potentially achieve a significant reduction in cost in comparison to currently available active mirrors.

The goal of this study is to develop a method to construct large ($>$ 1 m dia.), low mass ($\sim$ 1 - 2 kg/m^2), deformable mirrors with large actuation capabilities (shape adjustment range on the order of millimeters). By incorporating such a large dynamic range in actuation, the tolerances on the initial manufacturing processes can be reduced from say, optical (10s of nm) to mechanical (10s - 100s of μm) as the mirror now has in-situ corrective capabilities. Furthermore, it is envisioned that these mirrors are to be suitable for applications ranging from concentrators for solar power generation to primary mirrors for optical telescopes.

The paper is arranged as follows. The next section presents an overview of the mirror components as well as a simple design relationship for sizing the active layer. Section III displays the expected performance of the mirror using numerical simulation techniques. Sections IV and V present work performed on the development and characterization of a prototype mirror. Conclusions are then presented in Section VI.

II. Mirror Concept and Realization

A. Mirror Substrate

The substrate of the mirror is to be stiff, lightweight and easy to manufacture. It is also desired to be thermally stable and have tailorable mechanical properties. Due to these requirements, CFRP was selected as the candidate material. In this study, multiple layers of unidirectional fibers that have been pre-impregnated with epoxy matrix are arranged in a specific laminate orientation in order to make up the mirror substrate. The arrangement of the individual layers, or laminas, along with the mechanical properties of the fibers and epoxy, ultimately determine the mechanical behavior of the laminate. Additionally, new carbon-fiber processing techniques have made available laminas with thicknesses on the order of 30 μm. This allows for greater variability in the laminate design while maintaining an overall thickness on the order of 200 - 300 μm.

B. Active Elements

In order to keep the mirror thin and lightweight, surface parallel actuation was selected for shape correction. In this scheme, a series of thin active elements are laminated to the back of the mirror substrate. Upon application of voltage to the electrodes on the active elements an in-plane strain will occur. Since the elements are bonded to the substrate and are offset from the neutral axis, this in-plane strain will in turn cause an overall out-of-plane deformation. This deformation mechanism is what allows for shape-correction of the active mirrors.

The material for the active elements must have a good combination of stiffness and actuation capabilities in order to provide enough force to deform the relatively stiff CFRP substrate. It must also be capable of being manufactured into relatively small thicknesses in order to maintain the lightweight nature of the active mirror. For the current method, it was selected to use lead-zirconate-titante (PZT) as the active material. PZT is a piezoelectric ceramic that has a long history of use in the actuator and sensor industries. Table 1 is a list of typical mechanical and piezoelectric properties for this material.[10] It can be seen that PZT is

Table 1. Typical properties of Lead-Zirconate-Titanate (PZT).

Density	5.5 - 8.0 g/cm^3
Elastic Modulus (in-plane)	40-100 GPa
Poisson's Ratio	0.35
Piezoelectric Constant (d31)	-50 - -210×10^{-12} m/V
Piezoelectric Constant (d33)	120 - 600 $\times 10^{-12}$ m/V
Maximum Free Strain	200 - 1000 $\times 10^{-6}$

relatively stiff and has a high piezoelectric coefficient. It can also be manufactured in a fairly wide variety of shapes and sizes. However, it is an extremely brittle material making it difficult to work with especially when in plate/thick-film form. It also exhibits a significant amount of non-linear and hysteretic behavior in its piezoelectric response which requires carefully selected control schemes.

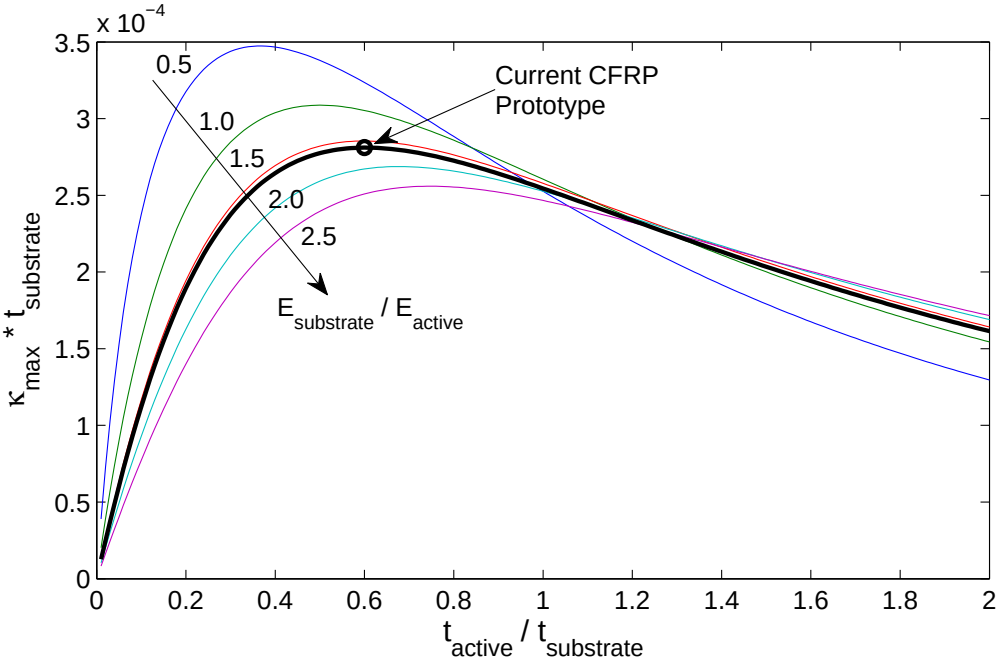

Figure 1. Variation of maximum curvature with thickness of active layer for different ratios of active layer to substrate thickness (κ_{max} corresponds to an applied active layer free-strain of 320 $\times 10^{-6}$.)

C. Laminate Design

Care must be taken in order to select the appropriate thickness and stiffness ratios between the mirror substrate and active material. While a thicker, stiffer active layer can apply more actuation force, it also increases the overall stiffness of the laminate, which can then decrease the actuation range of the mirror. In order to determine the optimal ratio of thicknesses, a preliminary study was performed based on Classical Lamination Theory (CLT).[11]

The in-plane strains and out-of-plane curvatures of a laminate are a function of actuation loads due to the piezoelectric strains of the active layer. They are defined as

$$\mathbf{N} = \mathbf{Q}_{active}\boldsymbol{\epsilon}_{active}t_{active} \tag{1}$$

$$\mathbf{M} = \mathbf{Q}_{active}\boldsymbol{\epsilon}_{active}\bar{z}_{active}t_{active} \tag{2}$$

where $\boldsymbol{N}$ and $\boldsymbol{M}$ are the in-plane forces and out-of-plane moments due to the active layer, $\boldsymbol{Q}_{active}$ is a 3×3 matrix containing the in-plane elastic properties of the active material, $\boldsymbol{\epsilon}_{active}$ is a 3×1 vector of piezoelectric strain components for the active material, $\bar{z}_{active}$ is the z-coordinate of the mid-plane of the active layer (with $z = 0$ corresponding to the mid-plane of the complete laminate), and t_{active} is the thickness of the active layer. Applying these loads to the complete laminate through its 6×6 stiffness ($\boldsymbol{ABD}$) matrix, the resulting in-plane strains, $\boldsymbol{\epsilon}$, and out-of-plane curvatures, $\boldsymbol{\kappa}$, are found from

$$\begin{bmatrix} \boldsymbol{\epsilon} \\ \boldsymbol{\kappa} \end{bmatrix} = \begin{bmatrix} \mathbf{A} & \mathbf{B} \\ \mathbf{B} & \mathbf{D} \end{bmatrix} \begin{bmatrix} \mathbf{N} \\ \mathbf{M} \end{bmatrix} \tag{3}$$

In order to find the maximum attainable curvature, $\boldsymbol{\kappa}_{max}$, the free-strain of the active material, $\boldsymbol{\epsilon}_{free}$ was used as the piezoelectric strain in Equations 1 and 2. Then, assuming the laminate to be symmetric ($\boldsymbol{B}= 0$), $\boldsymbol{\kappa}_{max}$ is given by

$$\boldsymbol{\kappa}_{max} = \mathbf{D}\mathbf{Q}_{active}\boldsymbol{\epsilon}_{free}\bar{z}_{active}t_{active} \tag{4}$$

Using this formulation, the material parameters of the active laminate can be varied and the corresponding changes observed. Figure 1 displays the results of this study. The maximum resulting curvature was calculated for a number of laminates with varying thickness and stiffness ratios. It can be seen that for a given stiffness ratio between the two materials, there is an optimal ratio of thicknesses in order to maximize the normalized out-of-plane deformation of the mirror. The expected behavior of a mirror constructed from a common CFRP substrate with an active layer of PZT is also plotted along with a point denoting the performance of the current prototype mirror, details of which are presented in Sections IV and V.

D. Fabrication Process

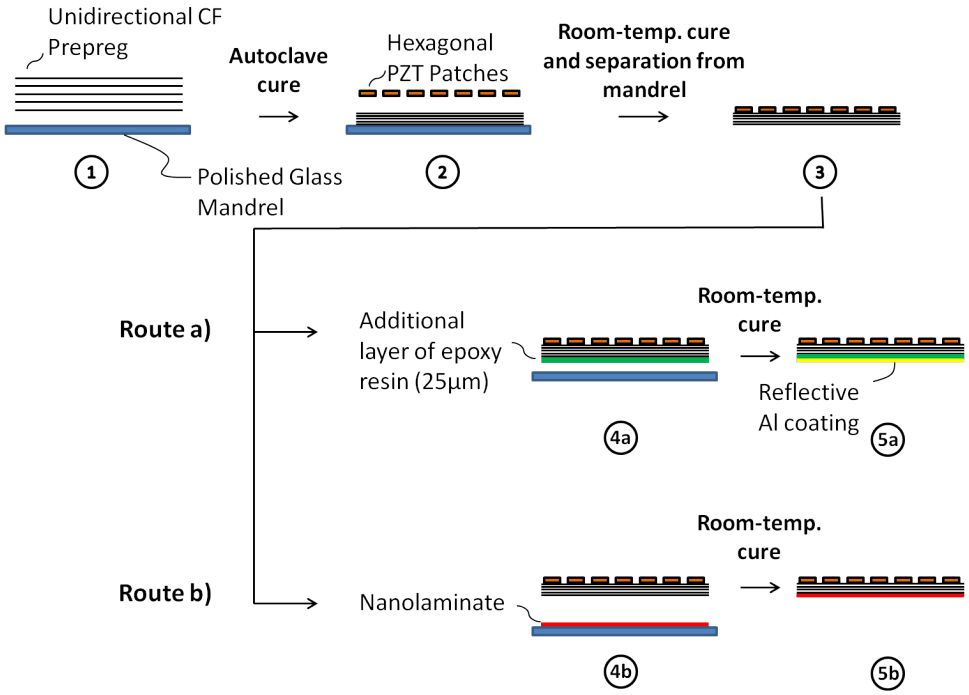

Figure 2. Schematic of mirror fabrication process.

Figure 2 is a schematic of the fabrication process for the proposed deformable mirror. First, a laminate consisting of plies of unidirectional carbon-fiber pre-preg is placed upon an optical-quality glass mandrel. The laminate is then vacuum bagged and processed in an autoclave under high-temperature and pressure in order to ensure consolidation of the carbon fibers. During this process, the epoxy resin becomes fluid-like and essentially 'flows' across the glass surface. Once cured, the outermost layer of epoxy will have replicated

the surface of the underlying polished mandrel, leaving a smooth reflective surface. Next, a series of piezoceramic actuators are arranged in a tessellation across the backside of the CFRP laminate in order to provide the desired actuation layer. They are bonded using a room-temperature cure process in order to mitigate any thermal distortions. In order to increase the surface finish of the mirror, two subsequent fabrication options have been considered. Option a) is to add an additional layer ($\sim$ 25 μm thick) of epoxy resin on the top surface of the laminate using a room-temperature cure in order to mitigate any residual defects not accounted for in the preliminary processes. A thin layer (100 nm) of aluminum is then vapor deposited over this surface in order to provide the reflective finish. Such a process has proven to be successful for carbon-fiber mirrors in the past.[12,13] Option b) is to bond a high-quality nanolaminate to the front surface of the mirror laminate in order to provide a smooth reflective surface.[3]

To date the majority of work has been devoted to process steps 1-3 in Figure 2 with work on subsequent surface finish improvements (steps 4-5) to be performed in the near future.

III. Expected Performance

In order to predict the expected performance of the mirrors, several numerical simulations were performed using Abaqus Standard 6.11. The mirror was modeled using elastic shell elements (S4) with quadratic interpolation and the material properties were defined using a composite stack lay-up. In order to model the linear piezoelectric response of the active layer, a thermal analog was used where an equivalent coefficient of thermal expansion was found by dividing the piezoelectric coefficient (d31) by the thickness of the PZT material. Using this method, the application of voltage to an actuator can be simulated simply by a temperature change.

The deformation corresponding to the actuation of a single actuator is known as the influence function of the actuator. These influence functions can be assembled into a matrix and, assuming linearity and independence between the actuators, this influence matrix can be used in a weighted least-squares formulation to find a voltage map in order to command the mirror to arbitrary shapes.[4] It should be noted that the assumptions of linearity in both the material response and the geometric nature of the problem are known to be of limited accuracy for PZT and very shallow shells. However, using this approach allows preliminary knowledge to be gained during the design process of the mirror laminates.

Figure 3 shows the results of a simulation used to model the potential corrective capabilities of the proposed mirrors. The simulation is of a 1 m diameter hexagonal mirror with a nominal radius of curvature of 15 m. The mirror is constructed from a 12-ply CFRP laminate (see Section V for the specific laminate orientation) and a 200 μm thick active layer with 96 independently addressable actuators arranged in a triangular tessellation. Through prototype development, it has been observed that relatively significant initial shape errors are present in the composite substrate prior to actuation. The most significant of these is a form of cylindrical deformation due to thermal stresses developed during the curing process. Therefore, the initial shape of the mirror model was set to have 5 mm of edge-to-edge cylindrical deformation on top of the nominal radius of curvature. This initial shape is shown in Figure 3(a). The influence functions of the mirror were then found and the corresponding voltage map was applied to each of the actuators in order to command the mirror to its base spherical shape. Figure 3(b) shows the result of this process where the mirror now has the approximate desired prescription. Figure 3(c) shows the residual shape error for the corrected mirror. It can be seen that the dominant source of error is due to the actuator print-through along the edges. The overall RMS error of the mirror is 52 μm which would be satisfactory for light concentrating applications. A finer pattern of actuators would be required in order to reduce this error for imaging applications.

On top of this initial correction process, the mirror can also be commanded to change its overall prescription. Figure 4 shows the resulting shape of the mirror when commanded to perform a net change of curvature. With a maximum applied voltage of 150V the mirror's radius of curvature can be changed from 15m to 11m. However, it can be seen that significant errors are introduced into the shape of the mirror due to the relatively coarse distribution of actuators.

IV. Prototype Mirror Development

Prototype mirrors have been developed in order to demonstrate the feasibility of the proposed concept. The mirrors are hexagonal in shape with a diameter of 150 mm (flat-to-flat) and a nominal initial radius of curvature of 2.5 m. They are constructed from ultra-thin carbon fiber laminas and thin plates of PZT.

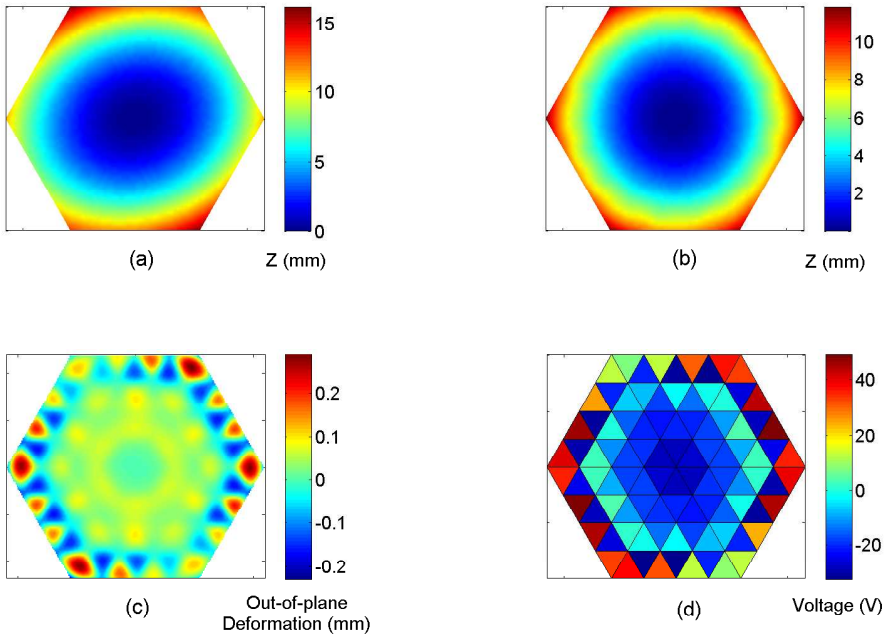

Figure 3. Simulation results of a 1 m diameter, hexagonal, CFRP mirror with 96 piezoelectric surface-parallel actuators showing (a) initial shape of mirror with significant cylindrical deformation (base R.O.C. = 15 m); (b) resulting mirror shape after correction; (c) corresponding surface residuals (RMS error = 52 μm); and (d) voltage map required to perform the correction.

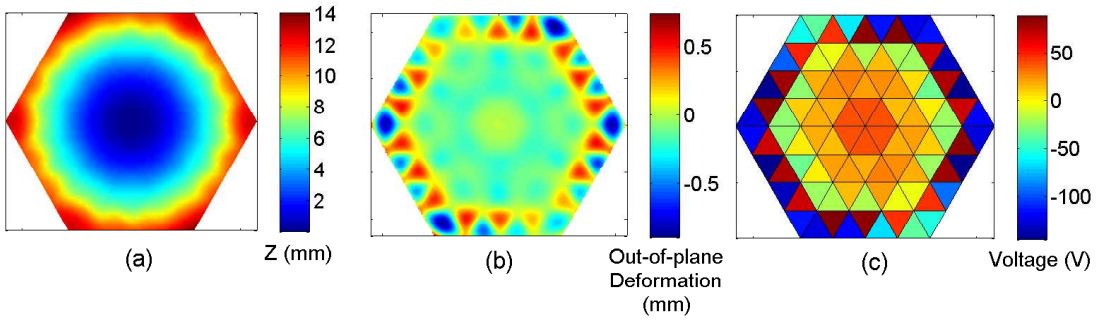

Figure 4. Attempted curvature change of simulated mirror with (a) resulting shape upon actuation (R.O.C. = 11 m); (b) corresponding residuals (RMS error = 161 μm); and (c) required voltage map (| V_{max} | = 150 V).

A. Thin-Ply Laminates

The ultra-thin carbon fiber composites are a product of North Thin-Ply Technologies®.[14] They are manufactured using a process called "spread-tow technology" where carbon fiber tows are simultaneously spread flat, impregnated with epoxy and combined together to form a unidirectional pre-preg tape. This process can produce tapes using virtually any form of carbon fibers and epoxy matrix. The tapes can be manufactured down to a fiber areal weight of 18 gsm while still maintaining high through-thickness uniformity. Figure 5 is a micrograph of the cross-section of an 8-ply laminate comprised of 30 gsm laminas arranged in a $[0^o/+45^o/\text{-}45^o/90^o]_s$ orientation. The laminate consists of T800 fibers impregnated by ThinPreg^{TM}120EPHTg-1 epoxy resin. It can be seen that there is a high-degree of uniformity between each lamina and a relatively uniform thickness of 28 μm (5-6 fibers) is maintained.

A full experimental characterization of the elastic properties of this material has been performed. Me-

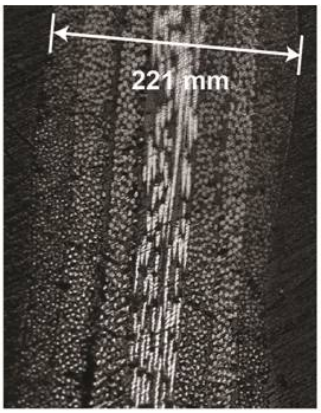

Figure 5. Micrograph of 8-ply laminate arranged in $[0^o/+45^o/\text{-}45^o/90^o]_s$ lay-up.

chanical tests were carried out on unidirectional specimens in order to characterize the orthotropic properties of a composite lamina. Loading was applied through an Instron 5500 Series materials testing machine with a 1000 N load cell. Deformations were captured using 3D Digital Image Correlation (DIC)[15] which produces full-field displacement and strain measurements. The results of these tests are presented in Table 2 where the 1-direction is parallel to the fibers and the 2-direction is perpendicular to the fibers. Using these results, along with Classical Lamination Theory, the mechanical properties of a laminate with arbitrary lamina orientation can be determined.

Table 2. Orthotropic properties of unidirectional T800 carbon fibers embedded in ThinPreg^{TM}120EPHTg-1 epoxy ($V_f \approx 50\%$).

Specimen	E_1 (GPa)	E_2 (GPa)	G_{12} (GPa)	ν_{12}
1	128.3	6.37	7.30	0.337
2	125.6	6.29	7.48	0.363
3	129.9	6.81	8.08	0.362
Average	**127.9**	**6.49**	**7.62**	**0.354**
% Variability	3.3	7.6	9.7	7.2

In order to provide the initial curvature for the mirror prototype, the CFRP laminate is cured on top of a polished glass mandrel with the intended mirror prescription. Prior to curing, the mandrel is coated with a non-particulate based release agent to aid in the release of the laminate. Once cured and removed from the mandrel, the bottom surface of the laminate produced by this process has a smooth, reflective surface as the epoxy matrix of the carbon fiber pre-preg has flown and replicated the surface of the underlying polished glass. Ideally, the surface of the mirror should completely replicate that of the glass mandrel. However, there are a number of factors that affect the surface finish of the mirror. The most prominent of these is due to fiber print-through. This is an expected source of error that is common in replicated CFRP mirrors[12,13,16] where upon cooling the relatively high CTE of the epoxy matrix causes it to contract around the carbon fibers. This behavior results in the fibers protruding out through the surface of the mirror and ultimately produces surface roughness with a wavelength on the order of the fiber spacing. Additional issues related to thermal stresses and irregularities in the carbon-fiber tapes also negatively affect the mirror surface finish.

Figure 6 is a Veeco Dektak Profilometer[17] measurement (with a 5 μm stylus radius) of the CFRP substrate. The measurement explicitly shows the effect of fiber print-through and its contribution to surface roughness. This effect has a wavelength on the order of the diameter of a single carbon fiber (~ 5 μm). It should be noted that the radius of the scanning stylus is approximately the same size as this characteristic wavelength, and therefore, several features may be missed with this test. Further tests will need to be performed in order to fully quantify the roughness of the laminate surface.

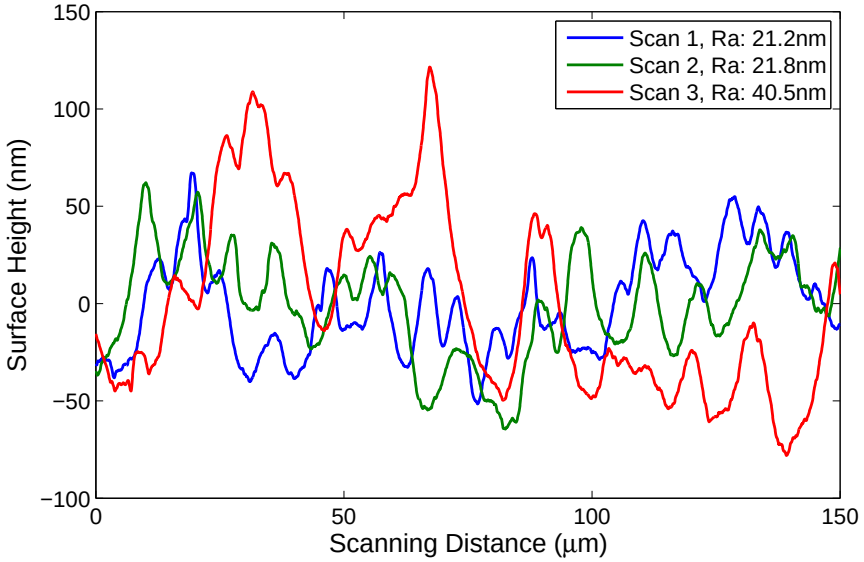

Figure 6. Veeco Dektak Profilometer measurement of CFRP surface depicting the effect of fiber print-through.

B. Active Layer

The active material used for the mirror prototype was obtained from Piezo Systems Inc.[18] Specifically, an industry type 5A (Navy Type II) PZT material was used. This class of PZT is characterized by having a relatively high piezoelectric constant, modest in-plane stiffness and is relatively insensitive to thermal effects. However, it is considered a 'soft' PZT, meaning that it has high domain mobility and is susceptible to depolarization at relatively low electric fields. Table 3 summarizes the mechanical and piezoelectric properties of this material.

Table 3. Mechanical and piezoelectric properties of PZT-5A.

Elastic Modulus (in-plane)	52 GPa
Poissons Ratio	0.3
Piezoelectric Constant (d31)	-190 x 10^{-12} m/V
Piezoelectric Constant (d33)	390 x 10^{-12} m/V
Coercive Field	1.2 x 10^{6} V/m

While PZT is a common material for actuators, its brittleness needs to be addressed before considering its use in the present application. Brittleness is of great importance to the present study as thin plates of PZT are to be bonded to the backside of a doubly-curved CFRP substrate. The magnitude of this initial curvature is enough to cause the PZT plates to fail and undergo brittle fracture.

In order to mitigate this problem, an extensive amount of work was performed in order to develop active layers that can be subjected to a large range of biaxial curvatures. It was found that this was possible to achieve by applying an initial pre-stress to the PZT material. The purpose of this pre-stress is to ensure that the PZT will remain in an entirely compressive stress-state even when deformed to relatively large curvatures. This ultimately reduces the occurrence of brittle fracture in the material thus expanding the range of suitable applications.

The pre-stress process, depicted in Figure 7, is achieved by laminating a PZT plate between two initially tensioned films of Kapton. This laminate of Kapton and PZT is then cured together under high-pressure using a thin layer of room-temperature cure epoxy. Once the epoxy has cured, the pre-tension in the Kapton films is removed. This in turn causes the laminated PZT to be subject to a compressive state of stress. The PZT/Kapton actuator can now be bent to large curvatures without fracturing, as seen in Figure 8. Currently, a compressive stress of approximately 30 MPa is applied to the PZT material. This allows the

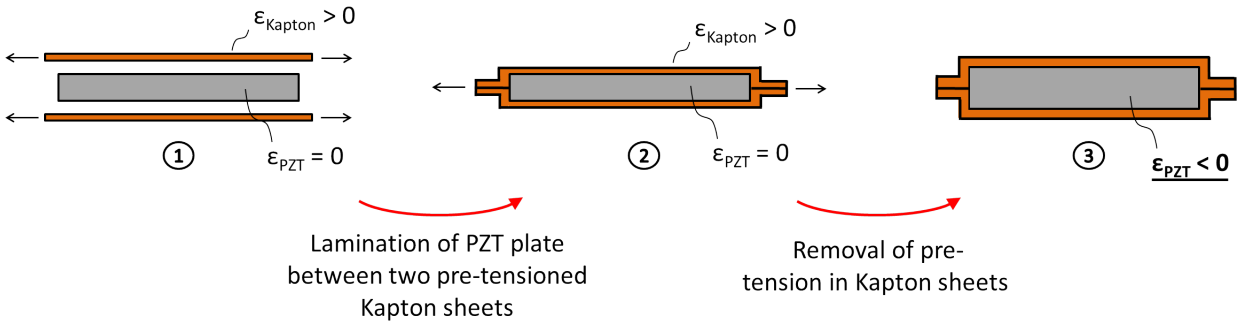

Figure 7. Schematic of active layer pre-stress process.

active layer to be bent to a biaxial radius of curvature less than 300 mm without fracturing. In addition to this, the pre-stress/lamination process also makes it possible for the actuators to be easily cut/trimmed into simple shapes depending on the application.

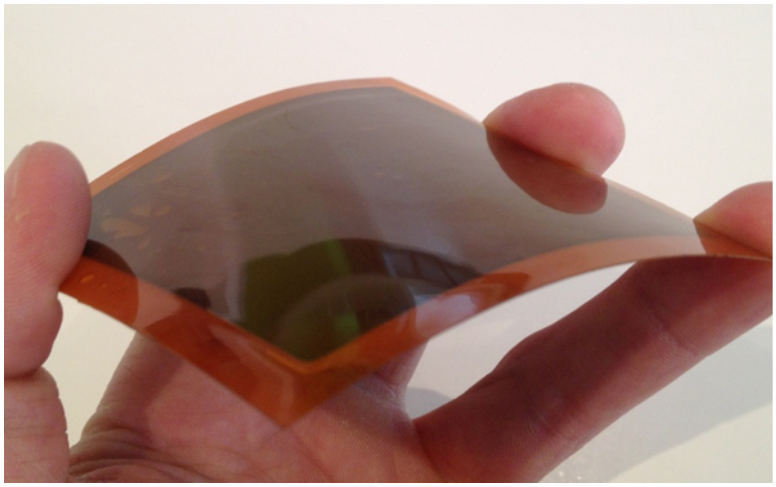

Figure 8. Demonstration of achievable curvatures for laminated actuators.

Using this process, several actuators were constructed and characterized. Figure 9 displays the piezoelectric response of these actuators when subjected to an electric field across the thickness of the PZT material. The first curve is the so-called "Butterfly Curve"[19] for the material which displays the entire piezoelectric response of the material across a large voltage range ($\pm$500 V). It can be seen that upon an initial application of voltage, the material undergoes an in-plane strain that is approximately linear with the applied voltage. Upon further application of voltage, this response starts to move into the non-linear regime. If the magnitude of applied voltage is increased enough such that the internal electric field exceeds that of the coercive field, ferroelectric switching will occur.[19] This is where the ferroelectric domains within the material switch orientation a full 180^o, essentially polarizing the material in the opposite direction. Once this occurs if the voltage is removed from the electrodes the material will follow a different path back to a zero strain-state. This path is now the new piezoelectric response of the material which is nearly symmetric to the previous state. It can be seen in Figure 9 that there is a slight amount of asymmetry to the butterfly curve which is attributed to remnant polarization of the material in its initial or preferred direction.

As ferroelectric switching is undesirable for most applications, understanding this behavior is essential in order to define practical operating conditions for the actuators. Figure 9 also displays the piezoelectric response of the material within a voltage range of $\pm$150 V. It can be seen that the piezoelectric strain of the material is now monotonically increasing (decreasing) when the voltage is applied in a certain direction. It can also be seen that there is a large amount of hysteresis associated with the piezoelectric response of the material. This effect complicates the use of the actuators as the response of the material is now dependent

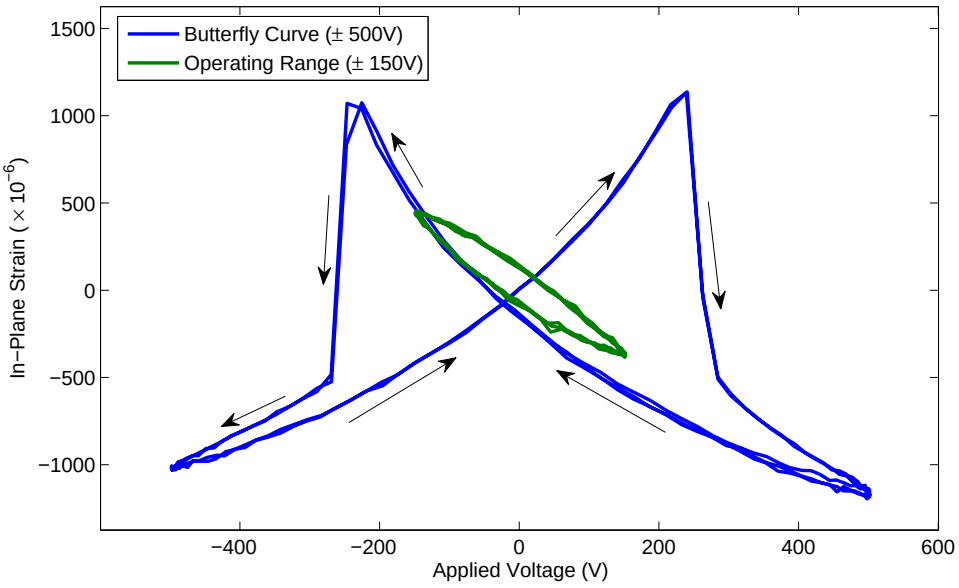

Figure 9. Piezoelectric response of active layer showing both the full-field strain response (butterfly curve at ±500 V) as well as the response under an operating voltage of ±150 V.

on its current and/or previous state. However, operational constraints can be put into place when applying voltage to the material in order to mitigate these effects. For example, a voltage "refresh" can be performed whenever a change is required where the actuator is first driven to a voltage lower than the intended value, held for a period of time, and then driven to its desired state. This ensures that the actuator is only operated in the "forward" direction, hence remaining on only one half of the operational curve shown in Figure 9.

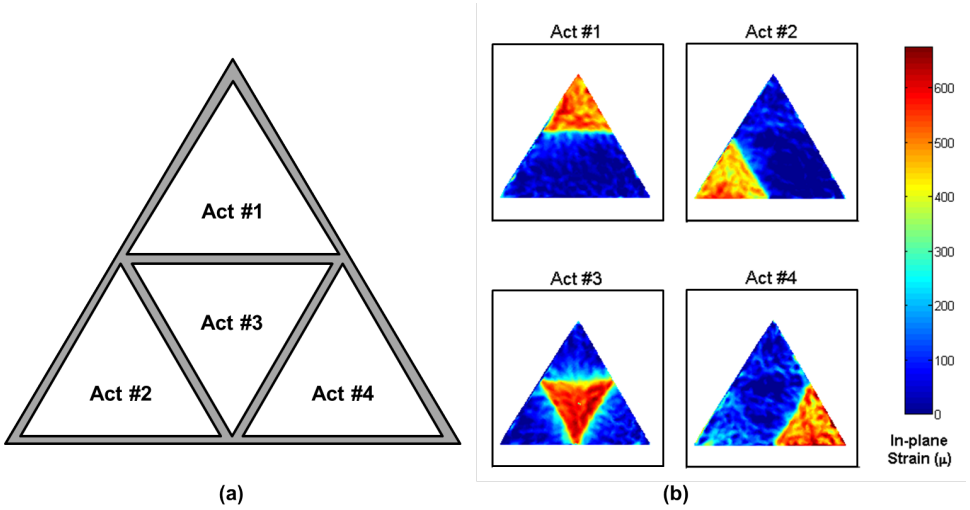

Figure 10. (a) Schematic of patterned electrode with four independent actuation regions and (b) corresponding in-plane strain in each region.

In order to increase the spatial control of the actuation scheme, work has also been performed in order to pattern the electrodes of the actuators and thus create independently addressable active regions across one plate of material. Patterning is done by selectively removing small portions of the electrodes on the surface of the PZT material, creating isolated regions with zero electrical conductivity between them. Electrical traces can then be routed to these newly formed regions where independent voltage values can be

applied. Figure 10(a) is a schematic of such a patterned actuator with four independently addressable regions. Figure 10(b) displays the corresponding in-plane strain measurements associated with these regions under an applied voltage of 150 V. It can be seen that there are distinct regions of strain corresponding to the addressable regions of the active element.

V. Current 150 mm Diameter Prototype

Figure 11 is a picture of the current active mirror prototype. It is constructed from a 12-ply laminate with a stack-up consisting of two consecutive layers of $[0^o/+60^o/\text{-}60^o]_s$. This particular laminate was chosen as it is symmetric (necessary to avoid large thermal distortions during curing) and has quasi-isotropic in-plane properties. It should also be noted that thinner (6-ply) laminates were used in previous studies, however they were susceptible to deformations due to inter-laminar stresses and boundary effects. Six triangular active segments are arranged in a regular tessellation across the backside of the mirror with a separation distance of approximately 2 mm. Each segment is 72.5 mm in side-length, 190 μm thick and patterned into four independently addressable regions providing 24 active channels in total. Voltage is applied to the electrodes on these regions via traces of thin copper wire which were incorporated during the lamination process.

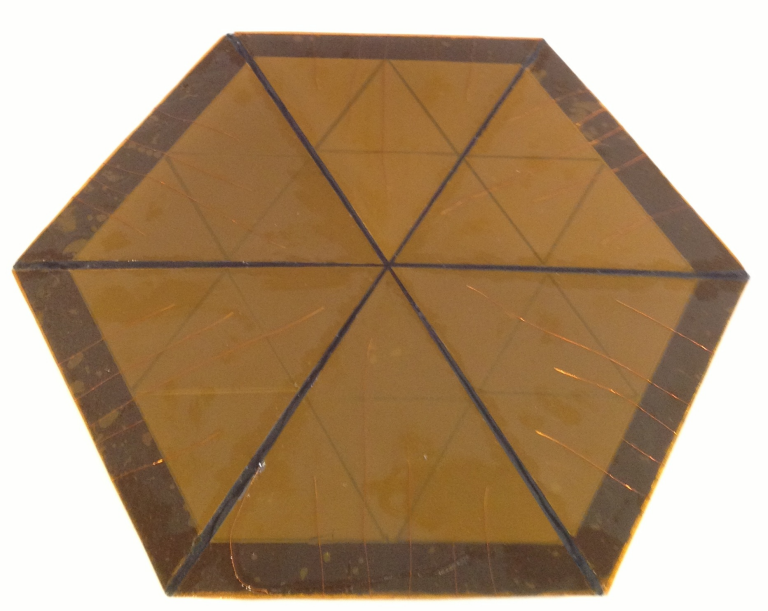

Figure 11. Current prototype mirror consisting of a 12-ply (two layers of $[0^o/+60^o/\text{-}60^o]_s$) CFRP laminate with 6 active segments bonded to its backside. Each active segment is patterned into 4 independently addressable regions with copper traces routed to each.

A. Characterization

In lieu of an optical test, 3D DIC was used to measure the influence functions of the mirror prototype. The resolution of the out-of-plane measurements was approximately 4 μm, which was adequate for the purposes of the preliminary characterization. Figure 12 shows the experimental set-up used to measure these influence functions. It can be seen that the mirror is held in a vertical orientation at 3 locations towards the edge of the mirror using small magnetic balls. As these spheres will automatically self-align with the flux lines of the magnetic field, they provide a simple way of achieving a kinematic mount without imposing localized distortions of the mirror surface.

The influence functions of the prototype mirror were also simulated numerically using the simulation techniques prescribed in Section III. In order to ensure good agreement between the simulations and experimental measurements it was necessary to develop a method of importing the initial prototype mirror shape into the simulations. To do this, the shape, or more specifically, a height map of the surface across the constructed prototype was measured and then through a simple interpolation process these height values

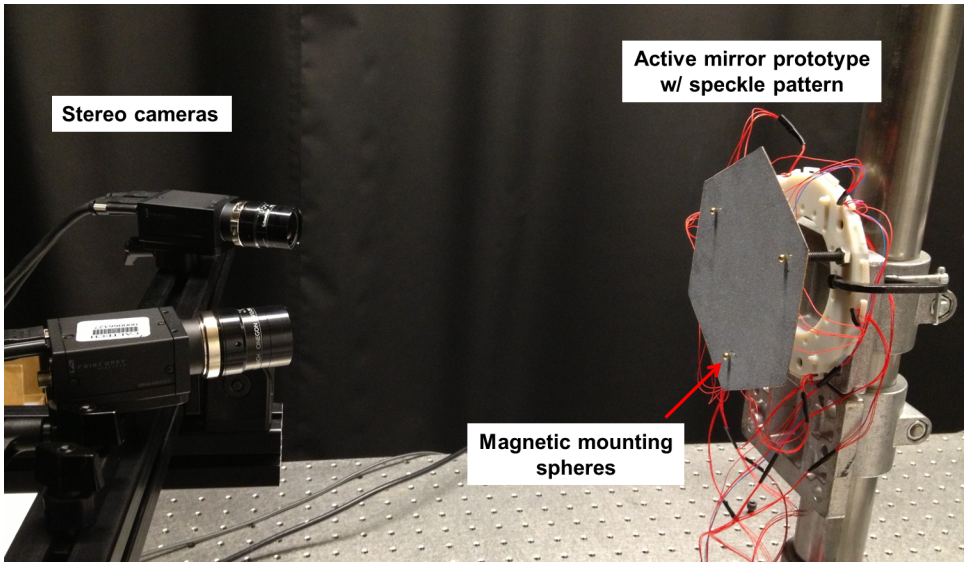

Figure 12. Experimental set-up used to measure influence functions of prototype mirrors.

were applied to the nodal coordinates of the mirror model. Once this was done, the numerical influence functions were found and compared to the experimental measurements.

Figure 13 displays the experimentally measured and the numerically derived influence functions for the prototype mirror when forcing each active segment to act as a single actuator (i.e. ignoring the patterned electrodes). It can be seen that the influence functions have both local and global features. The local response is characterized by a highly curved region in the approximate shape of the triangular actuator. The global response can be thought of as the 'decay' of this local response across the surface of the mirror. It can also be seen that there is good qualitative agreement between the experimental and numerical results. However, the magnitude of the influence functions (the peak-to-valley deformation per volt) does not match between the experiments and simulations. It is believed that this is due to inaccurate knowledge of 1) the thickness of the epoxy between the CFRP and active layer and 2) the piezoelectric properties of the active layer once bonded to the CFRP substrate.

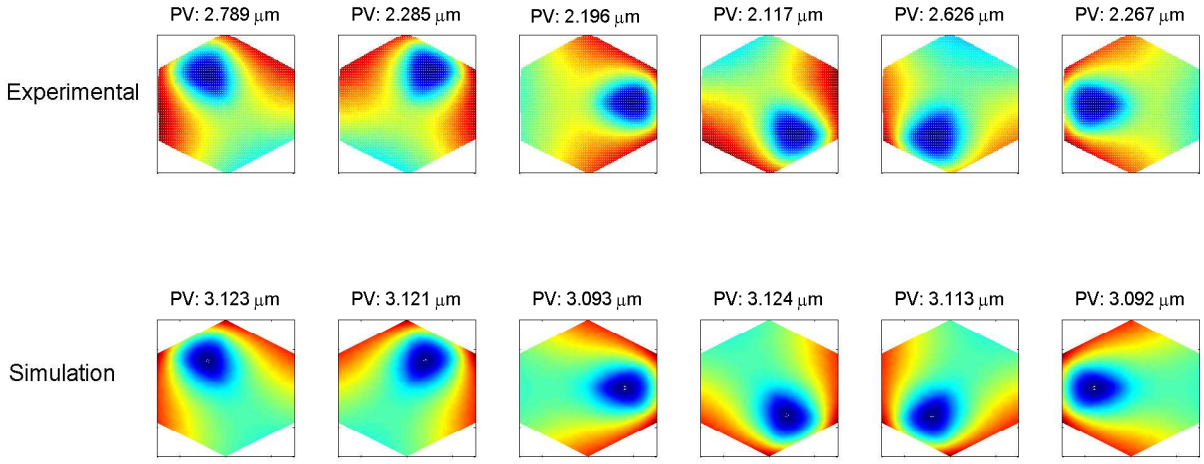

Figure 13. Experimentally measured and simulated influence functions with corresponding peak-to-valley (PV) deformations per volt. Each influence function corresponds to the 6 active segments of the mirror set to the same voltage.

Figure 14 displays the influence functions for the unique patterned regions of the active elements. It can

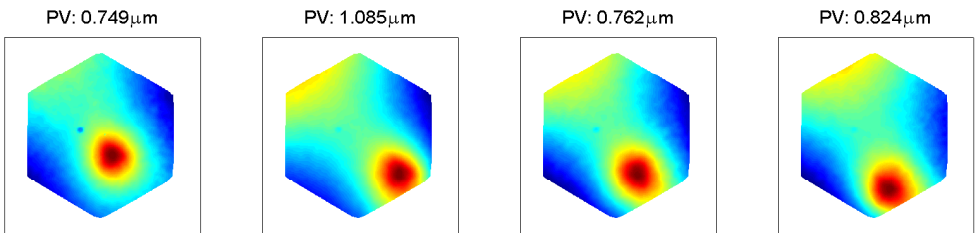

Figure 14. Examples of measured influence functions for patterned regions of an active segment.

be seen that these influence functions are smaller in size due to the reduced size of the active regions. This ultimately results in higher spatial control over the mirror surface. It should be noted the current prototype contains only 15 independent actuators. This was due to quality-control issues in the actuator patterning process which resulted in non-zero conductivity between several of the actuation channels, effectively causing them to act as one.

B. Prototype Performance

Figure 15 displays the shape correction capabilities of the current prototype mirror. It can be seen in Figure 15(a) that there is a significant amount of initial cylindrical deformation in addition to the base radius of curvature of 2.5 m. Figure 15(b) is the corrected shape once the mirror is commanded to return to the nominal spherical shape. It can be seen that there is a relatively significant improvement in the mirror figure. However, due to the limited number of independently working actuators in this prototype, residual errors remain. A total of 1.7 mm of peak-to-valley deformation was achieved during this correction process.

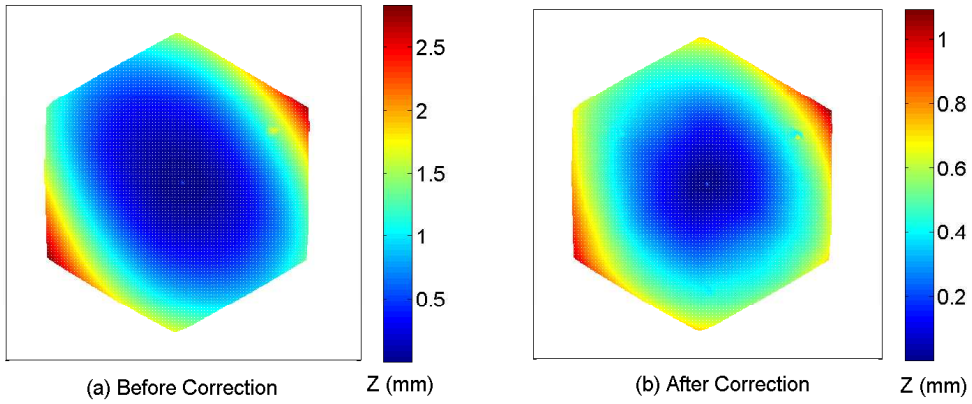

Figure 15. Shape correction capabilities of preliminary prototype mirror.

VI. Conclusions

The concept of an active mirror consisting of CFRP laminates and active segments of piezo-ceramic material has been developed. Preliminary studies related to obtaining an optical-quality surface as well as the actuation scheme have been performed. Small-scale prototype mirrors have been constructed using these techniques and characterized. Initial tests show that the prototypes exhibit significant potential to correct for initial shape errors in the mirror figure however, further refinement of the concept is needed in order to be suitable for practical applications.

Acknowledgements

We thank Gilles Rocher and Thomas Ricard (North Thin-Ply Technologies) for providing materials for this research and Professor Paolo Ermanni (ETH Zurich) for advice on actuator concepts and development. We also thank Keith Patterson (Caltech) for advice regarding the fabrication processes. Financial support has been provided by the Dow Resnick Bridge program at Caltech and the Natural Sciences and Engineering Research Council of Canada.

References

[1]H.P. Stahl, "Design Study of 8 Meter Monolithic Mirror UV/Optical Space Telescope." *SPIE: Space Telescopes and Instrumentation* 7010 (2008).

[2]J.P. Gardner, J.C. Mather, M. Clampin, et. al. "The James Webb Space Telescope." *Space Science Reviews* 123.4: 485-606. (2006).

[3]Hickey, G., Barbee, T., Ealey, M., Redding, M. "Actuated Hybrid Mirrors for space telescopes." *SPIE: Space Telescopes and Instrumentation* 7731 (2010).

[4]Patterson, K., Pellegrino, S. "Shape Correction of Thin Mirrors in a Reconfigurable Modular Space Telescope." *SPIE: Astronomical Instrumentation* 7731-72 (2010).

[5]Patterson, K., Pellegrino, S., Breckinridge, J. "Shape Correction of Thin Mirrors." *AIAA Structures, Structural Dynamics and Materials (SDM) Conference* (2011).

[6]Patterson, K., Yamamoto, N., Pellegrino, S. "Thin Deformable Mirrors for a Reconfigurable Space Telescope." *AIAA Structures, Structural Dynamics and Materials (SDM) Conference* (2012).

[7]Horne, S., McDonald, M., Hartsoch, N., Desy, K. "Reflective Optics CPV Panels Enabling Large Scale, Reliable Generation of Solar Energy Cost Competitive with Fossil Fuels." *National Renewable Energy Laboratory, Subcontract Report* (2009).

[8]Schipper, R., Makinen, J.T. "Injection Molding for Solar Concentrators." (2007).

[9]Cool Earth Solar. www.coolearthsolar.com (2013).

[10]PI (Physik Instrumente) L.P. www.piceramic.com (2012).

[11]Jones, R. M., "Mechanics of Composite Materials," 2nd ed. (1998).

[12]Hochhalter, J. D. "Replicated Mirrors Using Carbon Fiber Reinforced Polymers. Master's Thesis, Univ. of New Mexico (2005).

[13]Chen, P. C., et. al. "Advances in Very Lightweight Composite Mirror Technology." *Journal of Optical Engineering* 39-9 (2000).

[14]North Thin Ply Technology LLC. www.thinplytechnology.com (2013).

[15]Correlated Solutions, Inc. www.correlatedsolutions.com (2010).

[16]Massarello, J., Welsh, J., Hochhalter, J., et. al. "Fiber Print-Through Mitigation Technique for Composite Mirror Replication." *Journal of Optical Engineering* 45-12 (2006).

[17]Veeco Instruments Inc. www.veeco.com (2013).

[18]Piezo Systems Inc. www.piezo.com (2013).

[19]Araujo, C., Scott, J., Taylor, G. "Ferroelectric Thin Films: Synthesis and Basic Properties." *Ferroelectricity and Related Phenomena.* Book 10 (1996).